Discharge and Deposition Characteristics of High-Power Impulse Magnetron Sputtering Using Various Target Materials

Bocong Zheng, Zhongzhen Wu, Suihan Cui, Shu Xiao, Liangliang Liu, Hai Lin, Ricky K. Y. Fu, Xiubo Tian, Feng Pan, and Paul K. Chu

***Abstract*— The discharge and deposition characteristics of high-power impulse magnetron sputtering using various target materials with different sputtering yields (Cu, Cr, Ti, and C) were analyzed by a plasma global model. The experimental discharge voltages and currents of various target materials were used as the input parameters of the model. The analysis reveals that the ionization fraction of the sputtered species decreases as increasing the sputtering yield, due to the electron temperature was reduced through the cooling effect of sputtered species. However, as the sputtering yield increases, the plasma density under a given discharge power density is increased and the self-sputtering runaway can be fully developed, resulting in a higher fraction of ion density in the form of metal ions in the ion deposition flux. For some high-sputtering yield materials, such as Cu and Cr, this fraction can be up to 95%.**

***Index Terms*— Carbon, chromium, copper, modeling, plasmas, sputtering, titanium.**

I. Introduction

HIGH-power impulse magnetron sputtering (HiPIMS) has been known as an emerging ionized physical vapor deposition technique in recent years [1], [2]. By applying a unipolar pulse with high-power density to the target, while keeping a low-pulse frequency and duty cycle to avoid overheating, a high-density plasma of up to 1×10^{19} m^{-3} could be achieved [3]. One of the excellent characteristics of HiPIMS discharges is the ability to generate highly ionized sputtered species, thus providing a high ion flux to the substrate [4], and improving the microstructure and property of deposited thin films [5], especially for the density, adhesion, and conformality [6]–[8].

When the applied voltage went beyond a critical threshold [9], the generation of the highly ionized sputtered species in HiPIMS discharges is accompanied by a self-sputtering runaway [10], during which the discharge current increased dramatically. It is well-investigated that during the HiPIMS discharge, a funnel-shaped plasma potential formed over the target racetrack could result in an electric field which traps the ions back to the target to induce the self-sputtering process [11], [12]. The degree of self-sputtering can be represented by defining a self-sputtering parameter [13], [14]

$$\Pi_{SS} \equiv \alpha\beta\gamma_{SS} \tag{1}$$

where α is the ionization probability of a sputtered atom, β is the probability of the ionized species to return to the target, and γ_{SS} is the self-sputtering yield of the target ions. As increasing the discharge power density, more sputtered species becomes ionized and the degree of self-sputtering is enhanced. For the target material with a high-sputtering yield, the ionized target species may sustain the sputtering process itself at sufficiently high-power densities (typically $> 1 kW/cm^2$), which is commonly known as "sustained self-sputtering" (SSS) with a criterion of $\Pi_{SS} = 1$ [2]. For the case of $\Pi_{SS} < 1$, the discharge operates at a partially self-sputtering condition and gas ions are required to sustain the sputtering process; for $\Pi_{SS} > 1$, a self-sputtering runaway occurs and the discharge current keeps increasing, until the discharge runaway is limited due to some physical limitations and the discharge operates at the SSS mode ($\Pi_{SS} = 1$), or the arc suppression mechanism of the power supply is triggered and the discharge voltage is switched off. The self-sputtering process has been experimentally investigated and numerically modeled in recent years [9], [14]–[16]. Anders *et al.* [9] have experimentally investigated the current-voltage-time characteristics of HiPIMS discharges of various target materials, and qualitatively analyzed the role of secondary electrons and multiply charged metal ions played in the self-sputtering [14]. Huo *et al.* [16] demonstrated a numerical research on the road to self-sputtering in HiPIMS by a plasma chemical model. Kozak [15] presented a model analysis of HiPIMS discharge of Cu at different target power densities from hundreds to thousands of W/cm^2. Brenning *et al.* [17] developed a unified

Manuscript received July 1, 2018; revised October 11, 2018; accepted November 27, 2018. Date of publication December 13, 2018; date of current version January 8, 2019. This work was supported in part by the Guangdong Science and Technology Research under Grant 2015B090927003, in part by the Shenzhen Science and Technology Research under Grant JCYJ20150828093127698, in part by the City University of Hong Kong Applied Research under Grant 9667122, and in part by the Strategic Research under Grant 7004644. The review of this paper was arranged by Senior Editor F. Taccogna. *(Corresponding authors: Zhongzhen Wu; Feng Pan.)*

B. Zheng, Z. Wu, S. Cui, S. Xiao, L. Liu, H. Lin, X. Tian, and F. Pan are with the School of Advanced Materials, Shenzhen Graduate School, Peking University, Shenzhen 518055, China (e-mail: bcong.zheng@gmail.com; zzwu@pkusz.edu.cn; 1301214524@sz.pku.edu.cn; 1401111569@sz.pku.edu.cn; 1501213832@sz.pku.edu.cn; linhai@pkusz.edu.cn; xiubotian@163.com; panfeng@pkusz.edu.cn).

R. K. Y. Fu and P. K. Chu are with the Department of Physics and Materials Science, City University of Hong Kong, Hong Kong 999077 (e-mail: apkyfu@cityu.edu.hk; paul.chu@cityu.edu.hk).

Color versions of one or more of the figures in this paper are available online at http://ieeexplore.ieee.org.

Digital Object Identifier 10.1109/TPS.2018.2884475

treatment of self-sputtering, process gas recycling, and runaway for HiPIMS discharges, and a strong influence of the self-sputtering yield on the operation of HiPIMS discharges is observed. This paper aims to further elucidate the influence of target material on the discharge and deposition characteristics of HiPIMS. In this contribution, the discharge processes with various target materials were numerically modeled by reproducing the corresponding discharge currents. Some of the discharge and deposition characteristics, such as the ionization fraction and the ion fraction in the form of metal ions, are obtained and compared with experimentally measured results.

II. Model Description

The model of HiPIMS discharges presented here was based on the global description of the discharge region and considering the particle balance of each species and the energy balance of the whole system, the details can be found elsewhere [18], [19]. This paper extends the model by adding a self-consistent description of self-sputtering related parameters; the details are discussed in the following.

The ionization probability α of a sputtered atom in its life cycle (from the generation by the sputtering out of the target to the loss by departing away from the discharge region) is difficult to define in a time-varying situation [16], however, can be considered from the perspective of particle balance. Recalling that all the sputtered species are lost in the form of neutral atoms or charged ions, namely, the ionization probability can be approximately equivalent to the ionization fraction of the sputtered species departing away from the discharge region

$$\alpha = \frac{(1-\beta_{M^+})\Gamma_{M^+}(S_{IR}-S_T)+\Gamma_{M^+}S_T}{(1-\beta_{M^+})\Gamma_{M^+}(S_{IR}-S_T)+\Gamma_{M^+}S_T+\Gamma_M(S_{IR}-S_T)} = 1-\frac{1}{(1-\beta_{M^+})\frac{\Gamma_{M^+}}{\Gamma_M}+\frac{\Gamma_{M^+}}{\Gamma_M}\frac{S_T}{S_{IR}-S_T}+1} \tag{2}$$

where Γ is the flux of sputtered species departing away from the discharge region, M and M^+ are the metal atom and metal ion, S_{IR} and S_T are the surface area of the discharge region and the contact area between the discharge region and the target, respectively. The term of $(1-\beta_{M^+})\Gamma_{M^+}(S_{IR}-S_T)$ in (2) represents the ion flux diffusing away to the surrounding environment, $\Gamma_{M^+}S_T$ is the ion flux to the target surface and $\Gamma_M(S_{IR}-S_T)$ is the flux of unionized sputtered species away from the discharge region.

The self-sputtering parameter Π_{SS} indicates the degree of self-sputtering and determines the discharge current variation when the metal ions are overwhelmingly dominant in HiPIMS discharges. However, at relatively low-power densities or at the beginning of a discharge, there is considerable gas ions involved in the sputtering process. The gas ion assistance may play a crucial role in the discharge runaway of low-sputtering yield materials such as carbon [10], which can amplify the discharge current at a relatively low Π_{SS}. With the gas ion assistance, the flux of sputtered species is $\Gamma_{Ar^+}\gamma_{Ar^+}+\Gamma_{M^+}\gamma_{M^+}$ instead of $\Gamma_{M^+}\gamma_{M^+}$, and one can define an effective self-sputtering yield

$$\gamma_{eff} = \frac{\Gamma_{Ar^+}\gamma_{Ar^+}+\Gamma_{M^+}\gamma_{M^+}}{\Gamma_{M^+}} \tag{3}$$

which reduces the effect of gas ion assistance to the self-sputtering process, where Γ and γ are the ion flux and the sputtering yield of gas and metal ions, respectively. γ_{eff} represents the average number of target atoms ejected from the target per incident target ion with the gas ion assistance, the ion flux of each species at a given time can be obtained self-consistently by the model operation. Similarly, an effective self-sputtering parameter Π_{eff} which includes the gas ion assistance can be defined as

$$\Pi_{eff} \equiv \alpha\beta\gamma_{eff}. \tag{4}$$

The effective self-sputtering parameter Π_{eff} represents the trend of variation of discharge currents with the gas ion assistance and can be regarded as an "amplification factor" of the discharge current when $\Pi_{eff} > 1$. Assigning the self-sputtering period τ as the time for one cycle of the sputtered species from sputtering out of the target to being ionized and returning to the target, and assuming the discharge current I is proportional to the ion density n_i, the effective self-sputtering parameter Π_{eff} can be derived from the discharge current as

$$\frac{dI}{dt} = (\Pi_{eff}-1)\frac{I}{\tau}. \tag{5}$$

The self-sputtering period τ includes the time of ionization, transport, and back attraction. The averaged ionization time of a sputtered species is

$$\tau_{iz} = \frac{1}{k_{iz}n_e} \tag{6}$$

where k_{iz} is the reaction coefficient of electron-impact ionization, n_e is the electron density, the transport, and back attraction time of the sputtered species are adopted as 0.7 and 0.5 μm, respectively [16].

Due to the potential drop up to 10%–20% of the applied discharge voltage across the discharge region in HiPIMS [12], [20], the ionized species would be back attracted if its remnant energy is not sufficient to overcome the potential drop, and the resulting return probability β could be quite high, in the range of 0.8–1 [16]. However, recent studies on the details of HiPIMS discharges demonstrated that there are high plasma density regions, also called "spokes," moving along the racetrack during HiPIMS discharges [21], [22]. Each of the high-density region holds an asymmetric potential hump, which can be considered like a watershed for the ionized species [23], repels the ions outside the hump away from the discharge region [24], and may result in a decreased β [25]. Here, the return probability β is derived self-consistently from (2) and (4) as

$$\beta = \frac{\frac{\gamma_{eff}}{S'}+\Pi_{eff}-\sqrt{\left(\frac{\gamma_{eff}}{S'}-\Pi_{eff}\right)^2-4\gamma_{eff}\Pi_{eff}\frac{\Gamma_M}{\Gamma_{M^+}}}}{2\gamma_{eff}} \tag{7}$$

where $S' = (1-S_T/S_{IR})$ is a geometry factor. Adopting this β into the model, the self-sputtering related parameters, i.e., the α, β, and Π_{SS} can be obtained.

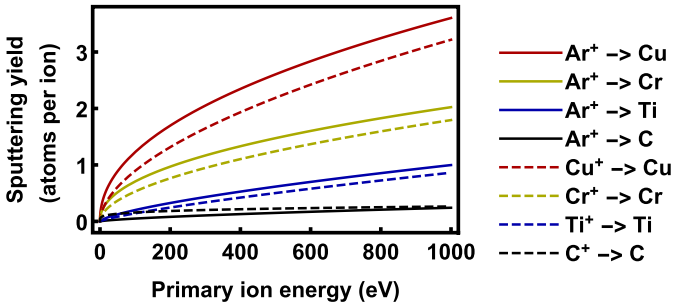

Fig. 1. Sputtering yields for Cu, Cr, Ti, and C as a function of ion bombardment energy.

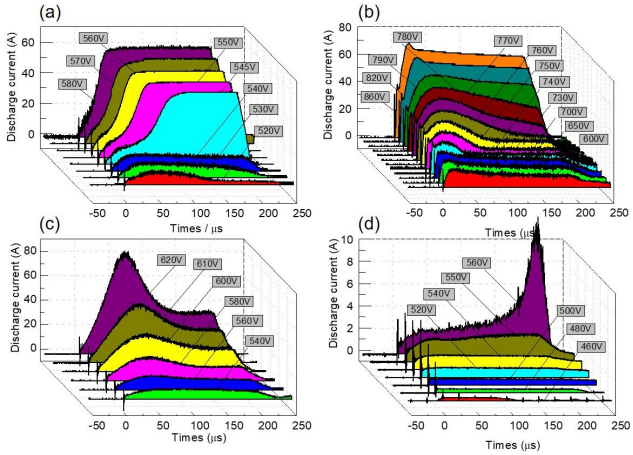

Fig. 2. Current–voltage–time characteristics of the HiPIMS discharge with a target of (a) Cu, (b) Cr, (c) Ti, and (d) C.

The sputtering yields by Ar ion bombardment and the self-sputtering yields for various target materials are demonstrated in Fig. 1, which are calculated by the Stopping and Range of Ions in Matter code [26]. In the voltage range used in this paper, Cu has the highest sputtering yield of more than two atoms per ion. For Cr, in the voltage range of 600–860 V, the sputtering yield is about 1.4 to 1.9. For Ti, the sputtering yield in the range of 540–620 V is about 0.6–0.7, however, since the second ionization energy of Ti species from Ti^{+} to Ti^{2+} (13.58 eV) is even lower than the ionization energy of Ar (15.76 eV), a large amount of Ti^{2+} species is expected and the self-sputtering yield by Ti^{2+} can be more than 1. The carbon species has the lowest sputtering yield of around 0.2.

III. Results and Discussion

To obtain the experimental discharge voltages and currents, four kinds of planar targets, Cu, Cr, Ti, and C were selected for the HiPIMS discharge experiments. The diameter of the targets is 2 in (5 cm) and the thickness is 4 mm. The base pressure is 1×10^{-3} Pa and the working gas is Ar of 99.999% purity at a pressure of 0.5 Pa. High-power unipolar pulses were supplied to the target using a home-made HiPIMS power supply [27]. The target current and voltage were monitored by a Tektronix TDS1012B-SC digital oscilloscope. Fig. 2 shows the current–voltage–time characteristics of the HiPIMS discharge with various target materials, the pulsewidth is 200 μs. Depending on the voltage, peak target current densities ranging from

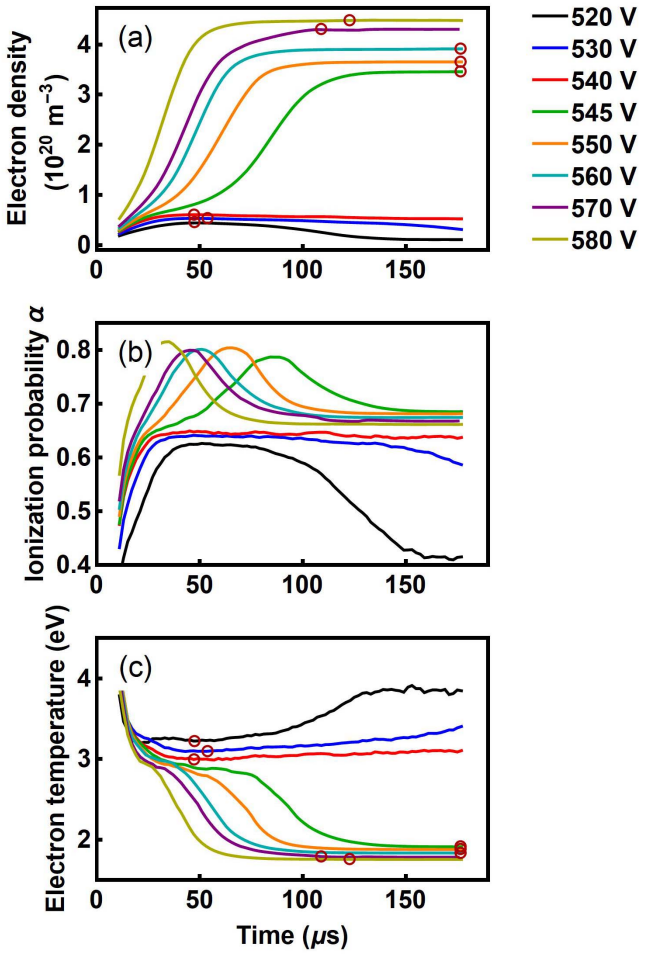

Fig. 3. Time evolutions of (a) electron density n_e, (b) ionization probability α, and (c) electron temperature T_e of Cu at different discharge voltages from 520 to 580 V.

1–8 A/cm^2 were obtained. These discharge current shapes were similar to the threshold demonstrated by Anders *et al.* [9]. For Cu discharges, above the threshold between 530 and 535 V, a plateau current is achieved. The discharge mode was switched from the partially self-sputtering to the SSS, between which an onset and a limitation of the self-sputtering runaway can be observed. For Cr discharges, a relatively high-sputtering yield can be achieved as the discharge voltage increases, the discharge current can almost reach a steady state, which indicates that the discharge state is near the SSS. For other target materials with a lower sputtering yield, no steady-state current can be achieved.

As an example of the calculation, some modeling results of Cu discharges are illustrated in Fig. 3, including the time evolution of the electron density, the ionization probability α, and the electron temperature at different discharge voltages from 520 to 580 V. The electron densities are proportional to the input power, therefore, have a similar profile to the discharge currents, as shown in Fig. 3(a). Fig. 3(b) shows that the ionization probability α increases dramatically at the initial period of the pulse at all voltages; below the voltage threshold of 545 V, α goes up to and maintains at about 0.6–0.65 as the time elapses during the pulses; above 545 V, α

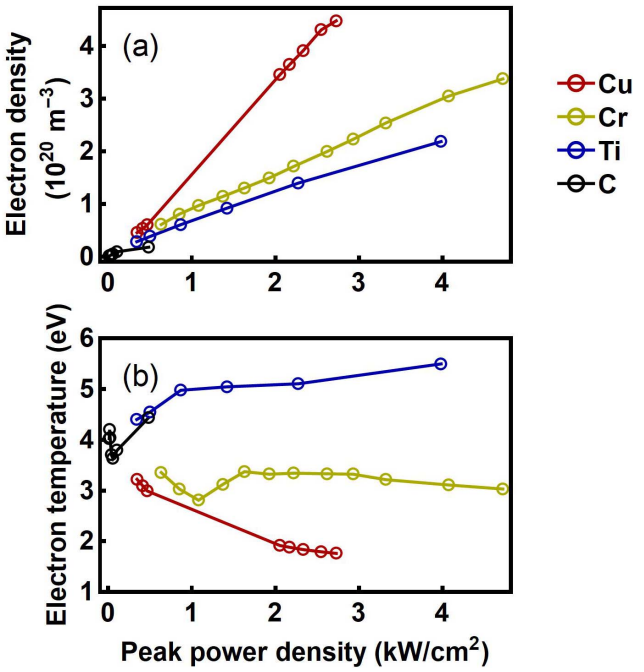

Fig. 4. Variation of (a) electron densities and (b) electron temperatures with peak power density for various target materials.

first increases to a peak value then drops and keeps at about 0.7, the steady-state value decreased slightly as increasing the discharge voltage. The α peaks appear above 545 V during the self-sputtering runaway phase should be attributed to the losses of target neutral species by the electron-impact ionization surpass the productions by the sputtering before the peak position, and vice versa after the peak due to the reduced ionization event. As illustrated in Fig. 3(c), the reduction of the ionization rate should be due to the increased supply of sputtered species during the self-sputtering runaway phases above 545 V, resulting in a cooling of the electron temperature T_e from 3 eV to around 2 eV. The slightly decrease of the steady state α as increasing the voltage could be explained similarly, which has already been predicted and observed [23], [28]. The red circles in Fig. 3(a) and (c) indicate the electron densities and temperatures under each discharge voltage at its maximum current. These values are used to describe the variation of discharge characteristics of Cu with power density in the rest of this paper, as well as other target materials.

The variations of electron density and temperature with power density for various target materials are summarized in Fig. 4. For each discharge voltage of each target material, the n_e and T_e at its maximum current are selected. The power density was averaged over the effective racetrack area S_T instead of the total area of the target. From Fig. 4(a), it can be clearly noted that the plasma density increases linearly with peak power density. This linear dependence has been observed in an HiPIMS discharge with Al target by Hecimovic *et al.* [29], indicating the applicability of describing the HiPIMS discharge by a simple global model. As the sputtering yield increases, the plasma density under a given discharge power density is increased, since there is an increase in the number of sputtered atoms that can be ionized. However,

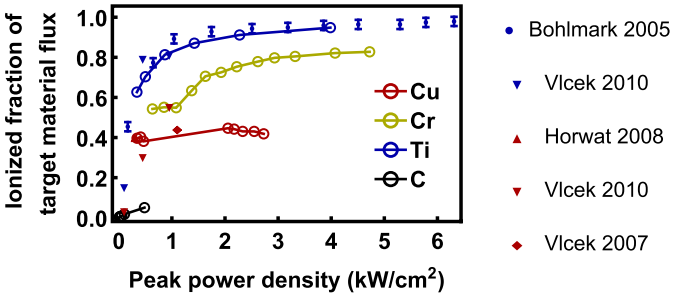

Fig. 5. Variation of ionized fraction of target material flux to the substrate with peak power density for various target materials.

the variation of T_e with peak power density shows a different tendency. For the target materials with a low-sputtering yield, C and Ti, T_e keeps increasing with the power density, since the sputtered species is not sufficient to cool the electrons. For Cr discharges, as increasing the discharge voltage, the flux of sputtered Cr atoms is increased, the corresponding cooling effect surpasses the enhanced heating effect caused by power increase, resulting in a decline of T_e. For Cu discharges, the cooling effect is even higher, leading to a significant reduction of T_e.

The ionized fraction of target material flux to the substrate is an important deposition characteristic which can significantly influence the microstructure and properties of deposited thin films [5]. In this model, it can be defined as

$$\Theta = \frac{\sum_i (1-\beta_i)\Gamma_i}{\sum_i (1-\beta_i)\Gamma_i + \Gamma_M} \tag{8}$$

where i are ions with various charge states. The variation of ionized fraction with the peak power density for various target materials is illustrated in Fig. 5, the data are selected in the same way as Fig. 4. To validate the modeling results, the experimentally measured values for Cu [30]–[32] and Ti [31], [33] were also demonstrated. The power density used in the model was averaged over the effective racetrack area, therefore, the power density adopted from the above-mentioned experimental results was converted to the same form, assuming these targets have a similar racetrack profile to the model. The ionized fraction decreases as the sputtering yield increases, except C, which has a much higher ionization threshold of 11.26 eV than other metals of 6.7–7.7 eV. The ionized fraction of Cu in the range of 0.5–3 kW cm^{-2} is around 0.4 and is little changed with the increase of the power density. For Cr discharges, the ionized fraction increases from less than 0.6 to around 0.8 in the range of 0.5–5 kW cm^{-2}, due to the higher electron temperature. The Ti discharge demonstrates an even greater ionized fraction, up to more than 95% under high-peak power densities, which is consistent with the experimental measurements by Bohlmark *et al.* [33]. The ionized fraction of C species is less than 0.1, due to the low-power density and high ionization energy of C atoms.

The fraction of metal ion current in the total ion current, i.e., the metal ion current fraction for various target materials is demonstrated in Fig. 6. Some experimental results are also summarized for Cu [31], [34] and Ti [31], [35], [36]. Similar trends can be observed by comparing the modeled and the

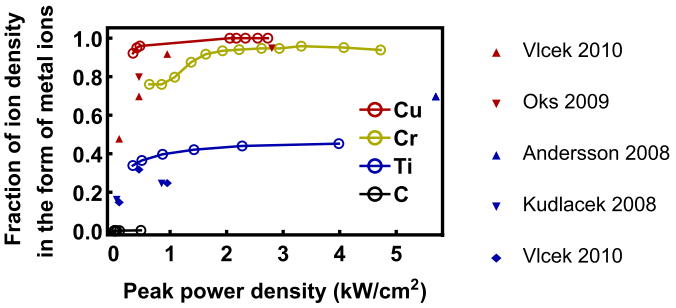

Fig. 6. Variation of ion fraction in the form of metal ions with peak power density for various target materials.

measured metal ion current fractions of Cu and Ti. The high-sputtering yield of Cu ensures a strong cooling effect on the electron temperature as the sputtered flux increased at high-power densities, therefore, the current amplification process can be limited by itself at sufficiently high-power densities and the transition to the SSS phase takes place. Once the discharge steps into the SSS mode, the discharge current is stabilized by a negative feedback. A disturbance to the higher discharge current leads to a higher sputtering and a stronger electron cooling effect, which results in a weakened ionization and offsets the initial fluctuation. The disturbance to the lower current is vice versa. During this phase, the discharge can be sustained by itself without the assistance of gas ions, resulting in a high metal ion current fraction. For other target materials with a lower sputtering yield, such as Ti, the supply of sputtered target species is insufficient to cool the electron temperature and regulate the ionization rate, a continuous runaway may take place until the amplification is stopped by the limitation of power supply [9]. The assistance of gas ions is required to sustain the recycling process [10], [17], and the metal ion current fraction could be significantly reduced. For C discharge, nearly all the ionized species in the ion flux are gas ions.

The parameters discussed earlier have an important significance in the HiPIMS discharges. Θ represents the ionized fraction of deposited flux, a high Θ ensures a high ion-to-neutral ratio of deposited species at the substrate surface, which is beneficial to the quality and adhesion of deposited thin films. The metal ion current fraction can nicely follow the variation of Π_{SS}, as demonstrated by Huo *et al.* [37]. A high Π_{SS} indicates a high purity of ion flux, which means there are less undesired gas ion in the deposition flux and the corresponding detrimental effect can be avoided. In an actual deposition process, the processing parameters need to be carefully selected according to the sputtering yield of target materials to obtain the desired properties of deposited thin films.

IV. Conclusion

In summary, the discharge and deposition characteristics of HiPIMS were studied by a plasma global model. The plasma parameters of HiPIMS discharges with various target materials (Cu, Cr, Ti, and C) are obtained, and some of the modeling results are compared with experimental measurements. The analysis reveals that the ionization fraction of the sputtered species decreases as increasing the sputtering yield. For low-sputtering yield materials, such as Ti, the ionization fraction can be up to 95% at high-peak power density of several kW cm^{-2}. For HiPIMS discharges with a Cu target, which has a high-sputtering yield, the ionization fraction can be reduced to around 0.4, due to the electron temperature was reduced through the cooling effect of sputtered species. However, as the sputtering yield increases, the plasma density under a given discharge power density is increased and the self-sputtering runaway can be fully developed, resulting in a higher fraction of the ion density in the form of metal ions in the ion deposition flux. For some high-sputtering yield materials, such as Cu and Cr, this fraction can be up to 95%. These results contribute to the understanding of the characteristics of HiPIMS discharges with various target materials, as well as provide a theoretical guidance for the parameters optimization in HiPIMS processing.

References

[1] V. Kouznetsov, K. Macák, J. M. Schneider, U. Helmersson, and I. Petrov, "A novel pulsed magnetron sputter technique utilizing very high target power densities," *Surf. Coat. Technol.*, vol. 122, nos. 2–3, pp. 290–293, 1999.

[2] J. T. Gudmundsson, N. Brenning, D. Lundin, and U. Helmersson, "High power impulse magnetron sputtering discharge," *J. Vac. Sci. Technol. A, Vac., Surf., Films*, vol. 30, no. 3, p. 030801, 2012.

[3] J. Alami, J. T. Gudmundsson, J. Bohlmark, J. Birch, and U. Helmersson, "Plasma dynamics in a highly ionized pulsed magnetron discharge," *Plasma Sources Sci. Technol.*, vol. 14, no. 3, pp. 525–531, 2005.

[4] J. Čapek, M. Hála, O. Zabeida, J. E. Klemberg-Sapieha, and L. Martinu, "Deposition rate enhancement in HiPIMS without compromising the ionized fraction of the deposition flux," *J. Phys. D: Appl. Phys.*, vol. 46, no. 20, p. 205205, 2013.

[5] A. Anders, "A structure zone diagram including plasma-based deposition and ion etching," *Thin Solid Films*, vol. 518, no. 15, pp. 4087–4090, 2010.

[6] M. Samuelsson, D. Lundin, J. Jensen, M. A. Raadu, J. T. Gudmundsson, and U. Helmersson, "On the film density using high power impulse magnetron sputtering," *Surf. Coat. Technol.*, vol. 205, no. 2, pp. 591–596, 2010.

[7] A. P. Ehiasarian, J. G. Wen, and I. Petrov, "Interface microstructure engineering by high power impulse magnetron sputtering for the enhancement of adhesion," *J. Appl. Phys.*, vol. 101, no. 5, p. 054301, 2007.

[8] H. L. Brown, S. A. Thornley, S. J. Wakeham, M. J. Thwaites, R. J. Curry, and A. M. Baker, "The impact of substrate bias on a remote plasma sputter coating process for conformal coverage of trenches and 3D structures," *J. Phys. D: Appl. Phys.*, vol. 48, no. 33, p. 335303, 2015.

[9] A. Anders, J. Andersson, and A. Ehiasarian, "High power impulse magnetron sputtering: Current-voltage-time characteristics indicate the onset of sustained self-sputtering," *J. Appl. Phys.*, vol. 102, no. 11, p. 113303, 2007.

[10] A. Anders, J. Čapek, M. Hála, and L. Martinu, "The 'recycling trap': A generalized explanation of discharge runaway in high-power impulse magnetron sputtering," *J. Phys. D: Appl. Phys.*, vol. 45, no. 1, p. 012003, 2011.

[11] A. Mishra, P. J. Kelly, and J. W. Bradley, "The 2D plasma potential distribution in a HiPIMS discharge," *J. Phys. D: Appl. Phys.*, vol. 44, no. 42, p. 425201, 2011.

[12] A. Rauch, R. J. Mendelsberg, J. M. Sanders, and A. Anders, "Plasma potential mapping of high power impulse magnetron sputtering discharges," *J. Appl. Phys.*, vol. 111, no. 8, p. 083302, 2012.

[13] A. Anders, S. Anders, M. A. Gundersen, and A. M. Martsinovskii, "Self-sustained self-sputtering: A possible mechanism for the superdense glow phase of a pseudospark," *IEEE Trans. Plasma Sci.*, vol. 23, no. 3, pp. 275–282, Jun. 1995.

[14] A. Anders, "Self-sputtering runaway in high power impulse magnetron sputtering: The role of secondary electrons and multiply charged metal ions," *Appl. Phys. Lett.*, vol. 92, no. 20, p. 201501, 2008.

[15] T. Kozák, "Effect of the target power density on high-power impulse magnetron sputtering of copper," *Plasma Sources Sci. Technol.*, vol. 21, no. 2, p. 025012, 2012.

[16] C. Huo, D. Lundin, M. A. Raadu, A. Anders, J. T. Gudmundsson, and N. Brenning, "On the road to self-sputtering in high power impulse magnetron sputtering: Particle balance and discharge characteristics," *Plasma Sources Sci. Technol.*, vol. 23, no. 2, p. 025017, 2014.

[17] N. Brenning, J. T. Gudmundsson, M. A. Raadu, T. J. Petty, T. Minea, and D. Lundin, "A unified treatment of self-sputtering, process gas recycling, and runaway for high power impulse sputtering magnetrons," *Plasma Sources Sci. Technol.*, vol. 26, no. 12, p. 125003, 2017.

[18] B. C. Zheng, D. Meng, H. L. Che, and M. K. Lei, "On the pressure effect in energetic deposition of Cu thin films by modulated pulsed power magnetron sputtering: A global plasma model and experiments," *J. Appl. Phys.*, vol. 117, no. 20, p. 203302, 2015.

[19] B. C. Zheng, Z. L. Wu, B. Wu, Y. G. Li, and M. K. Lei, "A global plasma model for reactive deposition of compound films by modulated pulsed power magnetron sputtering discharges," *J. Appl. Phys.*, vol. 121, no. 17, p. 171901, 2017.

[20] A. Mishra, P. J. Kelly, and J. W. Bradley, "The evolution of the plasma potential in a HiPIMS discharge and its relationship to deposition rate," *Plasma Sources Sci. Technol.*, vol. 19, no. 4, p. 045014, 2010.

[21] A. Anders, "Self-organization and self-limitation in high power impulse magnetron sputtering," *Appl. Phys. Lett.*, vol. 100, no. 22, p. 224104, 2012.

[22] A. P. Ehiasarian *et al.*, "High power impulse magnetron sputtering discharges: Instabilities and plasma self-organization," *Appl. Phys. Lett.*, vol. 100, no. 11, p. 114101, 2012.

[23] A. Anders, "Discharge physics of high power impulse magnetron sputtering," *Surf. Coat. Technol.*, vol. 205, pp. S1–S9, Jul. 2011.

[24] A. Anders, M. Panjan, R. Franz, J. Andersson, and P. Ni, "Drifting potential humps in ionization zones: The 'propeller blades' of high power impulse magnetron sputtering," *Appl. Phys. Lett.*, vol. 103, no. 14, p. 144103, 2013.

[25] J. Andersson and A. Anders, "Self-sputtering far above the runaway threshold: An extraordinary metal-ion generator," *Phys. Rev. Lett.*, vol. 102, no. 4, p. 045003, 2009.

[26] J. F. Ziegler, M. D. Ziegler, and J. P. Biersack, "SRIM—The stopping and range of ions in matter (2010)," *Nucl. Instrum. Methods Phys. Res. B, Beam Interact. Mater. At.*, vol. 268, nos. 11–12, pp. 1818–1823, 2010.

[27] Z. Wu *et al.*, "Novel plasma immersion ion implantation and deposition hardware and technique based on high power pulsed magnetron discharge," *Rev. Sci. Instrum.*, vol. 82, no. 3, p. 033511, 2011.

[28] L. Meng, H. Yu, M. M. Szott, J. T. McLain, and D. N. Ruzic, "Downstream plasma transport and metal ionization in a high-powered pulsed-plasma magnetron," *J. Appl. Phys.*, vol. 115, no. 22, p. 223301, 2014.

[29] A. Hecimovic, J. Held, V. Schulz-von der Gathen, W. Breilmann, C. Maszl, and A. von Keudell, "Probing the electron density in hipims plasmas by target inserts," *J. Phys. D: Appl. Phys.*, vol. 50, no. 50, p. 505204, 2017.

[30] D. Horwat and A. Anders, "Spatial distribution of average charge state and deposition rate in high power impulse magnetron sputtering of copper," *J. Phys. D: Appl. Phys.*, vol. 41, no. 13, p. 135210, 2008.

[31] J. Vlček and K. Burcalová, "A phenomenological equilibrium model applicable to high-power pulsed magnetron sputtering," *Plasma Sources Sci. Technol.*, vol. 19, no. 6, p. 065010, 2010.

[32] J. Vlček, P. Kudláček, K. Burcalová, and J. Musil, "High-power pulsed sputtering using a magnetron with enhanced plasma confinement," *J. Vac. Sci. Technol. A, Vac., Surf., Films*, vol. 25, no. 1, pp. 42–47, 2007.

[33] J. Bohlmark, J. Alami, C. Christou, A. P. Ehiasarian, and U. Helmersson, "Ionization of sputtered metals in high power pulsed magnetron sputtering," *J. Vac. Sci. Technol. A, Vac., Surf., Films*, vol. 23, no. 1, pp. 18–22, 2005.

[34] E. Oks and A. Anders, "Evolution of the plasma composition of a high power impulse magnetron sputtering system studied with a time-of-flight spectrometer," *J. Appl. Phys.*, vol. 105, no. 9, p. 093304, 2009.

[35] J. Andersson, A. P. Ehiasarian, and A. Anders, "Observation of Ti^{4+} ions in a high power impulse magnetron sputtering plasma," *Appl. Phys. Lett.*, vol. 93, no. 7, p. 071504, 2008.

[36] P. Kudláček, J. Vlček, K. Burcalová, and J. Lukáš, "Highly ionized fluxes of sputtered titanium atoms in high-power pulsed magnetron discharges," *Plasma Sources Sci. Technol.*, vol. 17, no. 2, p. 025010, 2008.

[37] C. Huo, M. A. Raadu, D. Lundin, J. T. Gudmundsson, A. Anders, and N. Brenning, "Gas rarefaction and the time evolution of long high-power impulse magnetron sputtering pulses," *Plasma Sources Sci. Technol.*, vol. 21, no. 4, p. 045004, 2012.

Authors' photographs and biographies not available at the time of publication.